

Ion collision cross sections and transport coefficients extended to intermediate energies and reduced electric fields for He_2^+ ions colliding with He

A. Chicheportiche,^{1,2,*} M. Benhenni,^{1,2} M. Yousfi,^{1,2} B. Lepetit,^{3,4} R. Kalus,⁵ and F. X. Gadea^{6,7}

¹Université de Toulouse, UPS, Laboratoire Plasma et Conversion d'Énergie, LAPLACE, Toulouse, France

²CNRS, UMR 5213, F-31062 Toulouse, France

³Université de Toulouse, UPS, Laboratoire Collisions Agrégats Réactivité, IRSAMC, Toulouse, France

⁴CNRS, UMR 5589, F-31062 Toulouse, France

⁵Centre of Excellence IT4 Innovations & Department of Applied Mathematics, VSB–Technical University of Ostrava, 17. listopadu 15/2172, 708 33 Ostrava, Poruba, Czech Republic

⁶Université de Toulouse, UPS, Laboratoire de Chimie et Physique Quantiques, IRSAMC, Toulouse, France

⁷CNRS, UMR 5626, F-31062 Toulouse, France

(Received 25 July 2013; published 23 October 2013)

This work is devoted to the calculation of transport coefficients for He_2^+ ions in gaseous He at intermediate reduced electric fields. These swarm data are of great interest for a better understanding of the mechanisms of formation and propagation of the fast plasma bullets or ionization waves observed in dielectric barrier plasma jet devices. For transport data, the collision cross sections required are determined from several theoretical methods based on quantum, semiclassical, and hybrid approaches and a diatomics-in-molecules model for the potential energy surfaces of He_3^+ . The corresponding collision cross sections are then used in an optimized Monte Carlo code to calculate the ion transport coefficients over a wide range of reduced electric fields extending over the experimental range. Calculated transport coefficients are compared with available experimental data at low electric fields. Moreover, an extrapolation method is used in order to determine the reduced mobility for stronger fields. A critical discussion has been performed on the pertinence and the reliability of these different methods of determination of collision cross sections needed for the calculation of ion transport data. Such ion data will be used in electrohydrodynamic and chemical kinetic models of the low-temperature plasma jet to quantify and to tune the active species production for a better use in biomedical applications.

DOI: [10.1103/PhysRevE.88.043104](https://doi.org/10.1103/PhysRevE.88.043104)

PACS number(s): 52.20.Hv, 51.50.+v, 52.25.Fi

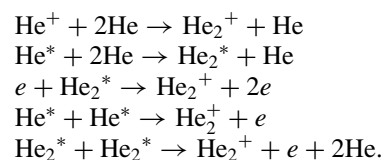
I. INTRODUCTION

Low-temperature plasma jets launched at atmospheric pressure can be initiated inside a cylindrical quartz tube wrapped by two thin alumina electrodes powered by a high voltage pulsed supply (see, e.g., Ref. [1]). In such a plasma device, the flowing helium gas is injected at low velocity (about 10 m/s) in the upstream side while the plasma jet propagates at much higher velocity (about 10^5 m/s) in the downstream side. Thus the plasma jet emerges in open air of several cm (around 4 cm) outside the glass tube. It was already shown that the continuous form of the observed plasma jet corresponds to a succession of fast bullets or ionization waves. The latter involves many active species (charged particles, radicals, long-lived excited species, photons, etc.) with a gaseous plasma temperature very useful for instance for living cell exposures since it generally remains lower than about 37°C [1]. The plasma active species are known to play a determinant role in many biomedical applications as for instance antitumor treatment, wound healing, blood coagulation, and others; Refs. [2] and [3] and the references given therein provide more information on this topic. The challenge for the plasma physics community is to tune such plasma device in order to abundantly or selectively produce some active species (atomic singlet oxygen, ozone, hydrogen peroxide, metastable helium, or hydroxyl, etc.) beforehand

identified for their bactericide, antitumor, or cell-regenerating effects.

Therefore, to optimize such plasma sources to each specific biomedical application it is very important to better understand the mechanisms of formation and propagation of the fast plasma bullets or ionization waves observed in the plasma jet devices. Electrohydrodynamic and chemical plasma models are in complement to experimental measurements very useful tools to study the physical phenomena and to accurately quantify the generated active species [1]. However, the use of such models required a good knowledge of ion swarm input data (reduced mobility, diffusion coefficients, and reaction rates) that are determined in the present work for diatomic helium ions.

As a matter of fact, in the case of electrical discharges using helium carrier gas at atmospheric pressure, the atomic and diatomic ions, He^+ and He_2^+ , can significantly affect the physical and chemical properties of the low-temperature plasma jet used in the biomedical field [4]. In fact, after the formation of atomic ions He^+ and metastable He^* in the plasma discharge by impacts with energetic electrons, He_2^+ molecular ions are rapidly formed in the atmospheric pressure devices following two-body or three-body, reactions [5]



*chicheportiche@laplace.univ-tlse.fr

As ionization waves in a low-temperature plasma jet propagate outside the discharge region mainly in helium when it is not yet diluted in ambient air [1], the electric field is mainly controlled by He_2^+ ions. This is why a good knowledge of He_2^+ ion transport coefficients is absolutely necessary to determine accurately the electric field self-generated by ionization waves and the abundance of the associated active species.

In weakly ionized gases under action of an external electric field, transport coefficients are closely related to the ion-neutral interaction potential curves and the corresponding collision cross sections. A previous study [6] determined the best *ab initio* interaction potential of the He^+/He interaction system in order to get the most accurate reduced mobility results of He^+ ions in He. Other He^+/He transport coefficients can be found in the literature (see, e.g., Ref. [7]). The purpose of this work is to compute transport coefficients of He_2^+ ions in He over a wide range of reduced electric field E/N (ratio of the electric field E over the gas density N). Mobility experimental data are available only for E/N lower than 25 Td (1 Td = 10^{-17} V cm²) while there are no data for diffusion coefficients and reaction rates. Reduced mobility has been determined from momentum transfer collision cross sections instead of differential cross sections [6] by using an optimized Monte Carlo code [8]. The collision cross sections have been obtained from a diatomics-in-molecules (DIM) model for the He_3^+ interaction potential [9,10]. These collision cross sections have been calculated using three different approaches, quantum, semiclassical, and hybrid methods, over a center-of-mass energy range varying from 1 meV to 40 eV.

The rest of the paper is organized as follows. Following this introduction, Sec. II is devoted to description of calculation methods of collision cross sections and of computation of ion transport coefficients. The diatomics-in-molecules interaction potential of He_2^+/He system [9,10] is first described. Then, the different calculation methods of collision cross sections are briefly reviewed. Quantum and semiclassical Jeffreys-Wentzel-Kramers-Brillouin (JWKB) methods [11] are described together with the infinite order sudden (IOS) approximation for the inclusion of vibrations and rotations of the He_2^+ molecule colliding with He atoms [12]. A hybrid molecular dynamics simulation, mixing quantum and classical dynamics taking explicitly into account vibrational and rotational motions is also presented. Then, a short description of the Monte Carlo simulation for the ion transport coefficients is given. Section III summarizes the results we obtained and is divided in four parts. The first part presents calculated collision cross sections and the corresponding ion reduced mobilities obtained with the quantum and semiclassical JWKB methods over a reduced electric field E/N range varying from 1 Td to 150 Td. A comparative analysis between the calculated reduced mobilities and available experimental data [13] is provided. The second part presents the results obtained with the hybrid molecular dynamics simulation and compares them to experimental results. Moreover, longitudinal and transversal diffusion coefficients useful for multidimensional fluid modeling of low-temperature plasma jet were also calculated using the method, which gives the best agreement with experimental results. The third part then reports the results obtained via a rigid core interaction potential model used to reproduce experimental reduced mobility at low reduced electric field

E/N and then to extrapolate them to higher fields up to 500 Td. Finally, we draw some discussions in Sec. IV.

II. METHODS AND COMPUTATIONS

A. Diatomics-in-molecules surfaces

In order to obtain potential energy surfaces for the He_2^+/He interaction system, the diatomics-in-molecules (DIM) methodology has been used. In short, the DIM method enables us to decompose the electronic Hamiltonian of He_n^+ clusters into a sum of atomic and diatomic contributions [14],

$$\hat{H}_{\text{DIM}} = \sum_{A=1}^{n-1} \sum_{B=A+1}^n \hat{H}_{\text{AB}} - (n-2) \sum_{A=1}^n \hat{H}_A, \quad (2.1)$$

where n is the total number of atoms in the cluster, A and B any of the atoms of the cluster, \hat{H}_{AB} the electronic Hamiltonian for the diatomic molecule, either He_2^+ or He_2 , and \hat{H}_A contains all electronic kinetic energy operators, which depend only on the atom A. If a diabatic basis set of n electronic wave functions representing states with the positive charge localized on a particular He atom is employed, the electronic Hamiltonian \hat{H}_{DIM} can be written in the form of an $n \times n$ real-valued matrix. The matrix elements can be expressed in terms of diatomic potential energy curves of the electronic ground state (Σ_u^+) and the first excited state (Σ_g^+) of He_2^+ and the electronic ground-state potential of He_2 . Atomic contribution leads to a global shift of the diagonal elements and can be set to zero. The diatomic inputs are usually provided by independent *ab initio* calculations. Since it is well known that the pure DIM model does not work well for helium cations larger than dimer [15] due to an insufficient inclusion of three-body interactions, several approaches have been proposed to improve its performance. They can basically be divided into two families: one employing explicit three-body corrections to the DIM Hamiltonian matrix [16,17] and another using empirical modifications of the diatomic potential energy curve for He_2 to effectively include the missing three-body effects [18]. In this work, a very recent model belonging to the latter family is used [9,10]. After diagonalization, the eigenvalues of the Hamiltonian matrix give the three adiabatic electronic levels of He_2^+/He interaction system. The collisional problem then involves three electronic channels (partners' internal states) with different asymptotic energies and charge distributions. Channel 1 and channel 2 correspond respectively to the two possible localizations of the positive charge: $\text{He}_2^+(\Sigma_u^+) + \text{He}(^1S)$ and $\text{He}_2(\Sigma_g^+) + \text{He}(^2S)$, and channel 3 corresponds to electronically excited ionic diatom, $\text{He}_2^+(\Sigma_g^+) + \text{He}(^1S)$.

B. Calculations of collision cross sections

1. Quantum and semiclassical methods

In the quantum and semiclassical approaches, in order to keep a minimum of degrees of freedom and simplify collision cross section calculations, the infinite order sudden (IOS) approximation [12] was used. In the framework of this approximation, the vibrational and rotational motions of the diatomic ion are neglected, i.e., the distance r_{fix} between the two He atoms of the He_2^+ molecule has been frozen.

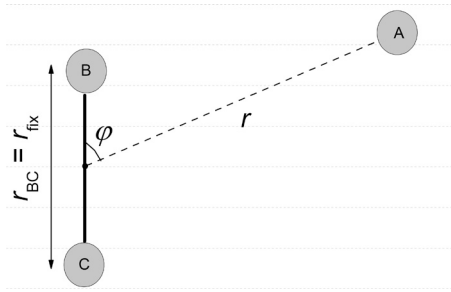


FIG. 1. Centre of mass coordinates used for collisions between the dimer BC (He_2^+) and the atom A (He). r_{fix} is the distance between the two helium atoms B and C and r is the distance between the centre of mass of the He_2^+ molecule and the third He atom. The approach angle φ is defined as the angle between the internuclear axis of He_2^+ and the axis between the centre of mass of the dimer and the He atom. $\varphi = 0^\circ$ corresponds to the linear trimer configuration (A, B and C being aligned).

The trimer orientation in space is described by the approach angle φ between the He^+ -He internuclear axis and the axis between the He_2^+ center of mass and the third helium atom, and by the distance r between the center of mass of the He_2^+ molecule and the helium atom (see Fig. 1 showing the center of mass coordinates used for the $\text{He}_2^+ + \text{He}$ collisions). This allows us to treat the anisotropic atom-molecule interaction potential as an atom-atom one for each approach angle φ and frozen diatomic internuclear distance r_{fix} . The anisotropy of the atom-molecule interaction is taken into account by a

simple average without weighting over the approach angle φ . We note n_φ the number of approach angles needed in order to obtain converged collision cross section value. In the two calculation methods, a number of approach angles $n_\varphi = 21$ was found sufficient in order to get converged collision cross section results. Figure 2 displays an overview on the adiabatic electronic ground state $V_1(r, \varphi; r_{\text{fix}})$ [Fig. 2(a)], first excited state $V_2(r, \varphi; r_{\text{fix}})$ [Fig. 2(b)] and second excited state $V_3(r, \varphi; r_{\text{fix}})$ [Fig. 2(c)] for He_2^+/He interaction system versus distance r for approach angles $\varphi = 0^\circ, 45^\circ, 90^\circ$ and for a frozen distance $r_{\text{fix}} = r_{\text{eq}} = 2.1$ a.u. (equilibrium distance of the He_2^+ molecule). Figure 2(d) shows the interaction potentials when the distance between the atoms of the diatomic r_{BC} varies and when the third atom A is at infinity. Potential energies at $r_{\text{BC}} = r_{\text{eq}}$ give the asymptotical energies of $V_1(r, \varphi; r_{\text{eq}})$, $V_2(r, \varphi; r_{\text{eq}})$, and $V_3(r, \varphi; r_{\text{eq}})$, respectively, shown in Figs. 2(a)–2(c) and respectively equal to about -2.45 eV, 1.5 eV, and 6.8 eV (origin of energies are then taken for the plateau $\text{He}^+ + \text{He} + \text{He}$). Therefore, electronically inelastic processes cannot take place for collision energies below about 4 eV.

We present now integral and momentum collision cross sections calculated with the quantum method. The problem is considered like an atom-atom one where the colliding partners can be in different internal states or channels. In order to get collision cross sections for elastic and inelastic processes, the diabatic electronic basis is used to perform the collision cross-section calculation.

The formalism used to compute collision cross sections is described in Ref. [19]. This general formalism is valid for

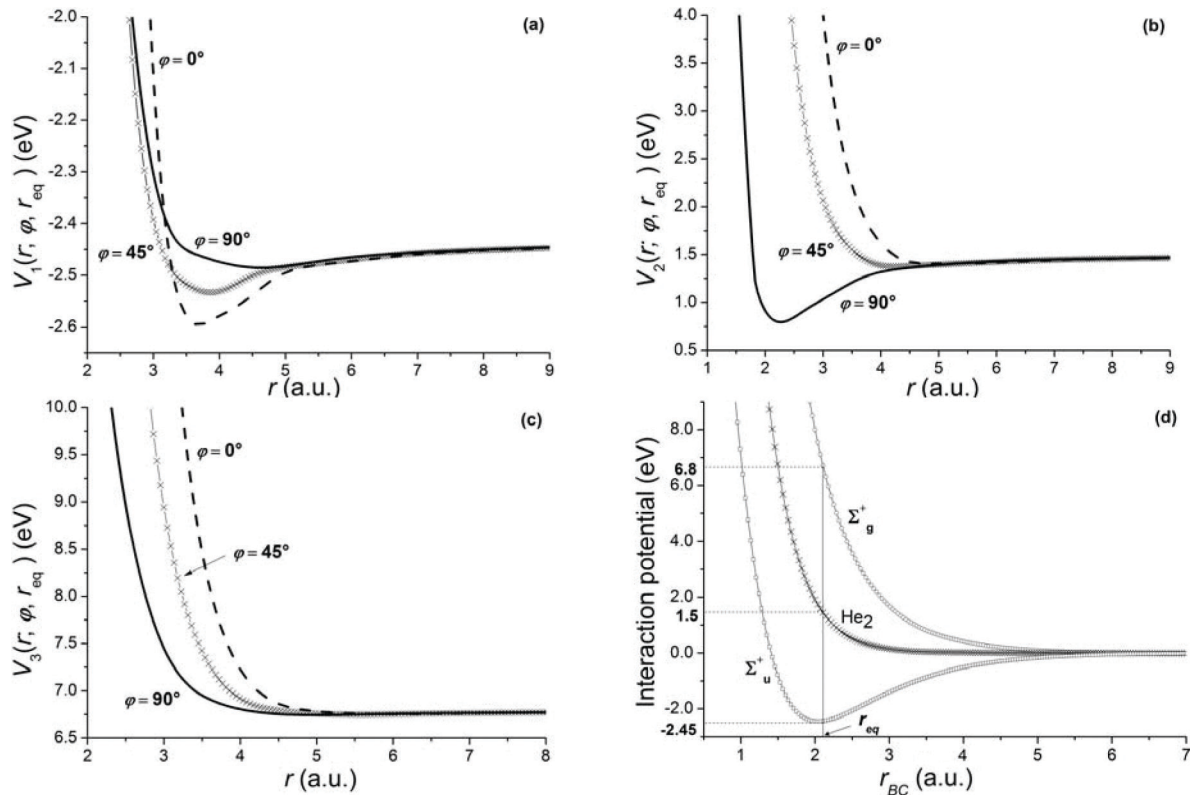


FIG. 2. Adiabatic electronic ground state (a), first excited state (b) and second excited state (c) for He_2^+/He interaction system versus internuclear distance r between He and He_2^+ for approach angles $\varphi = 0^\circ, 45^\circ, 90^\circ$ and for a fixed distance $r_{\text{fix}} = r_{\text{eq}} = 2.1$ a.u. between the two atoms of the diatomic ion. Figure (d) shows the interaction potential when the distance $r \rightarrow \infty$ and when r_{BC} varies.

elastic and inelastic processes. Using partial wave expansion with angular momentum l , the integral cross section $Q_0^{ij}(\varepsilon; r_{\text{fix}}, \varphi)$ and the momentum transfer cross section $Q_1^{ij}(\varepsilon; r_{\text{fix}}, \varphi)$ at collision energy ε from initial channel i to final one j for a given r_{fix} and φ are given by

$$\begin{aligned} Q_0^{ij}(\varepsilon; r_{\text{fix}}, \varphi) &= \frac{\pi}{k_i^2} \sum_l (2l+1) |T_{ij}^l(\varepsilon; r_{\text{fix}}, \varphi)|^2 \\ Q_1^{ij}(\varepsilon; r_{\text{fix}}, \varphi) &= \frac{\pi}{k_i^2} \sum_l (2l+1) |T_{ij}^l(\varepsilon; r_{\text{fix}}, \varphi)|^2 - 2(l+1) \text{Re} \\ &\quad \times [T_{ij}^l(\varepsilon; r_{\text{fix}}, \varphi)^* T_{ij}^{l+1}(\varepsilon; r_{\text{fix}}, \varphi)], \end{aligned} \quad (2.2)$$

where k_i is the initial wave vector, $T_{ij}^l(\varepsilon; r_{\text{fix}}, \varphi)$ is a transition matrix element and Re refers to the real part of the product of transition matrix elements. Transition matrix is obtained by integration from a short distance r_{min} in the classically forbidden region to a large one r_{max} where the wave functions can be matched to the asymptotic ones (typically Bessel functions), following the procedure outlined for instance in Ref. [19].

The problem involves three channels with different asymptotic energies. The 3×3 transition matrix provides three collision cross sections, $Q^{11}(\varepsilon; r_{\text{fix}}, \varphi)$ for the elastic process ($\text{He}_2^+ + \text{He} \rightarrow \text{He}_2^+ + \text{He}$), $Q^{12}(\varepsilon; r_{\text{fix}}, \varphi)$ for the charge exchange one ($\text{He}_2^+ + \text{He} \rightarrow \text{He}_2 + \text{He}^+$) and $Q^{13}(\varepsilon; r_{\text{fix}}, \varphi)$ for incident ion excitation ($\text{He}_2^+ + \text{He} \rightarrow \text{He}_2^{*+} + \text{He}$). The transition matrix is obtained by a simple numerical integration from r_{min} to r_{max} over the corresponding potential using the De Vogelaere algorithm [20]. We typically used $r_{\text{min}} = 0.5$ a.u and $r_{\text{max}} = 100$ a.u. The integration was performed with 20 points per wavelength. Moreover, collision cross sections were also calculated using only the first adiabatic electronic state $V_1(r; \varphi; r_{\text{fix}})$, in order to analyze inelastic charge transfer and incident ion excitation processes impact on elastic collision cross sections and on calculated reduced mobilities.

Semiclassical elastic collision cross sections can also be obtained as previously [cf. Eq. (2.2)] but by using the semiclassical collisional phase shifts. Indeed, there is a simple expression for the transition matrix for a given r_{fix} and φ as a function of the collisional phase shifts $\delta_l^{\varepsilon; r_{\text{fix}}, \varphi}$ by $iT^l(\varepsilon; r_{\text{fix}}, \varphi) = 1 - e^{2i\delta_l^{\varepsilon; r_{\text{fix}}, \varphi}}$ [19]. However, contrary to the symmetrical systems, such as He^+/He [6], there is no expression that allows us to obtain inelastic charge transfer collision cross sections. In this method, the semiclassical JWKB approximation [11] has been used to calculate phase shifts from the first adiabatic electronic state $V_1(r; \varphi; r_{\text{fix}})$. These phase shifts are determined as a function of the collision impact parameter b and the interaction potential $V_1(r; \varphi; r_{\text{fix}})$, i.e.,

$$\begin{aligned} \delta_l^{\varepsilon; r_{\text{fix}}, \varphi} \approx \delta^{\varepsilon; r_{\text{fix}}, \varphi}(b) &= k_i \int_{r_0^{\varphi; r_{\text{fix}}}}^{\infty} \left[1 - \left(\frac{b}{r}\right)^2 - \frac{V_1(r; \varphi; r_{\text{fix}})}{\varepsilon} \right] dr \\ &\quad - k_i \int_b^{\infty} \left[1 - \left(\frac{b}{r}\right)^2 \right] dr, \end{aligned} \quad (2.3)$$

where $b = (l + 1/2)\hbar/k_i$ and $r_0^{\varphi; r_{\text{fix}}}$ represents the distance of closest approach for $V_1(r; \varphi; r_{\text{fix}})$.

For the transport coefficients calculation, required quantum $Q_1^{ij}(\varepsilon; r_{\text{fix}})$ or semiclassical $Q_{1, \text{JWKB}}^{11}(\varepsilon; r_{\text{fix}})$ momentum transfer cross sections are then obtained by integration over solid angle, which corresponds here to a simple average of $Q_1^{ij}(\varepsilon; r_{\text{fix}}, \varphi)$ or $Q_{1, \text{JWKB}}^{11}(\varepsilon; r_{\text{fix}}, \varphi)$ respectively over the approach angle φ .

2. Hybrid method

In the hybrid approach, the heavy nuclei are treated classically and follow a trajectory while the potential is computed using the time-dependent Schrödinger equation, and decoherence is taken into account periodically. Appropriately initial conditions need to be generated appropriately and the equations of motion integrated numerically to evaluate the momentum transfer cross section.

The He_2^+/He collision complex has been treated semiclassically [21] using the Ehrenfest mean-field approach with classical equations of motion for nuclei,

$$\dot{q}_l = \frac{p_l}{M_l}, \quad \dot{p}_l = -\langle \psi | \frac{\partial \hat{H}_{el}}{\partial q_l} | \psi \rangle \quad (2.4)$$

and the quantum Schrödinger equation for electrons,

$$i\hbar \frac{\partial \psi}{\partial t} = \hat{H}_{el} \psi. \quad (2.5)$$

Here, q_l and p_l denote respectively nuclear coordinates and momenta of each atom of mass M_l , ψ is current electronic wave function, \hat{H}_{el} represents electronic Hamiltonian [in this work $\hat{H}_{el} = \hat{H}_{\text{DIM}}$ of Eq. (2.1)], and $\langle \cdot | \cdot \rangle$ denotes the usual scalar product on the electronic Hilbert state space (i.e., integration over all electronic coordinates). Since the method mixes classical and quantum approaches, we call it the *hybrid method* throughout this study. Within the DIM approach, Eqs. (2.4) and (2.5) transform to a matrix form if an appropriate basis set is used in the electronic state space. Following the usual practice (cf. Sec. II A), real-valued diabatic wave functions representing electronic states with the positive charge localized on a particular atom, φ_j , have been used. This finally leads to [21]

$$\dot{q}_l = \frac{p_l}{M_l}, \quad \dot{p}_l = -\sum_{j,k} a_j a_k \frac{\partial H_{jk}}{\partial q_l}, \quad i\hbar \dot{a}_j = \sum_k H_{jk} a_k, \quad (2.6)$$

where a_j and a_k are expansion coefficients of current electronic wave function with respect to the diabatic basis set, $\psi = \sum_j a_j \varphi_j$, and $H_{jk} = \langle \varphi_j | \hat{H}_{el} | \varphi_k \rangle$. This set of ordinary differential equations has been solved numerically in the center-of-mass system of the collision complex using a fourth-order Runge-Kutta algorithm. The integration step ranging between 0.01 fs and 0.1 fs (depending on the collision energy) has been used. Total integration times have been set sufficiently long so that the collision fragments are able to separate into a distance at which the interactions between them become negligible with respect to the collision energy. Typically, integration times of 0.5 ps through several dozens of picoseconds have been sufficient, depending again on the collision energy.

It has been shown previously [22] that quantum decoherence may be important in dynamical calculations if excited electronic states are involved. In the present work, it has

been included via a modified Mean Field with Quenching-Amplitude/Scaling (MFQ-AMP/S) method of Ref. [22]. Briefly, the quenching probabilities for a transition from a current electronic state to one of accessible adiabatic states have been calculated using adiabatic amplitudes of the current electronic wave function ψ . The nuclear momenta have been adjusted after each accepted electronic quenching by a simple multiplicative scaling so that the total energy of the collision system is conserved. Since the original MFQ-AMP/S approach does not conserve the total angular momentum of the nuclei unless it is zero [22], the velocity scaling procedure has been modified so that the angular momentum conservation law is obeyed even for nonzero total angular momentum. More specifically, the nuclear velocities are first transformed to a rotating coordinate system in which the total angular momentum of the colliding nuclei is zero and then scaled using the S method of Ref. [22]. Finally they are transformed back to the (inertial) center-of-mass system of the collision complex to be involved in further evolution.

The initial conditions consist, for the present task, of initial values of nuclear coordinates, momenta, and the initial electronic state of He_2^+ , and initial coordinates and momenta of the impacting neutral atom. The initial configurations of He_2^+ have been generated via microcanonical Monte Carlo simulations used to model vibration excitations of the dimer or simply by using a particular interatomic distance in frozen-dimer calculations. Then, a random rotation of the dimer ensuring its isotropic orientation in space has been employed. The initial momenta of the dimer atoms have been set, for each particular configuration, so that the total vibrational energy of the dimer is equal to the preselected value. The helium dimer has been assumed in its electronic ground state. The initial position of the He atom has been calculated from the initial distance between He and He_2^+ along the collision axis and from the particular value of the collision impact parameter. Distances along the collision axis ranging between 20 Å and 40 Å have been used depending on the collision energy. Values of the impact parameter have been generated randomly between $b_{\min} = 0$ Å and $b_{\max} = 3\text{--}16$ Å, the upper limit depending again on the collision energy, and weighted properly so that the He flux is homogeneous. The initial translational velocities in the He_2^+ /He center-of-mass system have been calculated from the center-of-mass collision energy.

Totally 20000–80000 trajectories have been calculated for each particular collision energy in order to get converged values of the collision cross sections. More trajectories are required for lower energies since higher maximum values of the impact parameter have to be used in that case. All the hybrid calculations have been performed using our MULTIDYN code package [23].

The hybrid calculations provide two collision cross sections: one denoted $Q_{1,\text{hyb}}(\varepsilon)$ and corresponding to elastic processes and electronic excitation processes not leading to the dimer dissociation, and another, $Q_{0,\text{hyb}}^{\text{diss}}(\varepsilon)$, related to the three-body dissociation ($\text{He}_2^+ + \text{He} \rightarrow \text{He}^+ + \text{He} + \text{He}$).

C. Calculations of transport coefficients

A Monte Carlo algorithm allows us to simulate the ion transport in a gas under the action of a uniform electric field E .

Detailed simulation techniques using the Monte Carlo method for transport coefficients calculation can be found elsewhere [8,24]. In short, the Monte Carlo code treats an initially great number of seed particles one by one until their disappearance when elastic and inelastic collisions are defined by their cross sections. In addition fictitious ionization (ion creation) is also considered in order to obtain more accurate results when there are large processes of ion removal such as asymmetric charge transfer or electron detachment. The usual approximation of a weakly ionized gas is made, where only interactions between ion and neutral species in their ground states are taken into account. This means that collisions between ion and excited neutral species are assumed negligible. The target gas motion at ambient temperature (300 K) has been taken into account in the calculation of the relative ion energy by considering both the ion and target gas velocities. Ion energy is calculated from the classical dynamics equations by considering the electric field acceleration and the energy of the target gas is determined assuming a Maxwellian distribution at 300 K.

Ion mobility data are then calculated from Monte Carlo simulation using the momentum transfer cross sections by assuming an isotropic scattering for the calculation of the deflection angle after every collision. As shown in a previous work [6], using this approximation, calculated transport coefficients present a maximal relative statistical deviation of $\pm 2\%$ from the calculated ones using the differential cross sections while gaining a factor of 20 in calculation time. Momentum transfer cross sections can be then considered as an approximation to indirectly take into account the anisotropy of collisions without using the differential cross section. In this case, the deviation angle θ is determined from a random number r_θ uniformly distributed in the interval [0,1] by the following relation:

$$\cos(\theta) = 1 - 2r_\theta. \quad (2.7)$$

The probability $P(t)$ of free time of flight t_{flight} between t_j (initial or last collision time) and t_{j+1} (collision time) is directly related to the momentum transfer collision cross section as follows:

$$P(t) = \exp\left(-\int_{t_0}^t \nu_{\text{tot}}(v(t')) dt'\right) \quad (2.8)$$

with ν_{tot} the total collision frequency given by,

$$\nu_{\text{tot}}[v(t)] = N v(t) Q_1[\varepsilon(t)], \quad (2.9)$$

where N is the gas density, Q_1 is the elastic or inelastic momentum transfer cross section and $v(t)$ and $\varepsilon(t)$ are respectively the time-dependent velocity modulus and energy. Free time of flight t_{flight} is then calculated using Eq. (2.8) from the logarithm of a random number. Ion trajectories $x(t), y(t), z(t)$ between two successive collisions are determined from classical equations where the electric field \vec{E} is applied along the z axis and accelerates uniformly the ions during their free flight.

Transport coefficients such as reduced mobility K_0 and longitudinal D_L or transversal D_T diffusion coefficients are determined respectively from the following relations:

$$K_0 N = \frac{\langle v_z \rangle}{E/N} \frac{T_0}{T_{\text{gas}}} \frac{P_{\text{gas}}}{P_0}, \quad (2.10)$$

$$D_L = \frac{1}{2} \frac{d[z(t) - \langle z(t) \rangle]^2}{dt}, \quad (2.11)$$

$$D_T = \frac{1}{4} \frac{d[(x(t) - \langle x(t) \rangle)^2 + (y(t) - \langle y(t) \rangle)^2]}{dt}, \quad (2.12)$$

where $T_0 = 273.16$ K is the standard temperature, T_{gas} is the gas temperature, $P_0 = 760$ torr is the standard atmospheric pressure and P_{gas} is the gas pressure. Considering a parameter X_{ij} related to the positive ion number i undergoing the collision number j during its drift towards the cathode under the action of the uniform electric field E , the mean quantity $\langle X \rangle$ is calculated by using a statistical mean from the conventional formula,

$$\langle X \rangle = \frac{1}{n_p} \sum_{i=1}^{n_p} \frac{1}{n_c} \sum_{j=1}^{n_c} X_{i,j}, \quad (2.13)$$

where n_p is the number of seed particles and n_c is the total number of collisions occurring during the whole ion pathway from its emission at the anode to its disappearance at the cathode. Such a definition is consistent with the uniform electric field condition and steady-state regime reached in the case of standard drift tube measurements for ion mobility [25].

III. RESULTS AND DISCUSSIONS

A. Quantum and semiclassical results

As the first step, we investigated the dependence of calculated collision cross sections and ion mobilities on the basis set. The previously described quantum method was used to calculate the elastic $Q_{0,1}^{11}(\varepsilon; r_{\text{fix}} = 2.1 \text{ a.u.})$, charge transfer $Q_{0,1}^{12}(\varepsilon; r_{\text{fix}} = 2.1 \text{ a.u.})$, and ion excitation $Q_{0,1}^{13}(\varepsilon; r_{\text{fix}} = 2.1 \text{ a.u.})$ collision cross sections from the diabatic Calvo's DIM interaction potential surfaces [9,10] with $r_{\text{fix}} = 2.1$ a.u. (cf. Sec. II A and Sec. II B1). Figure 3 shows the calculated momentum transfer cross sections for the elastic and charge transfer processes. The momentum transfer cross section for particles going from channel 1 to channel 3 (electronic excitation of ionic dimer) is not shown in Fig. 3 since it was found to be negligible. The inelastic ion excitation cross section is then negligible compared to the other ones and therefore has no significant effect on the ion mobility. As noted before, we see that the charge exchange process does not occur for relative energies ε below around 4 eV. Consequently, such charge transfer process does not affect the calculation of ion transport coefficients at low reduced electric fields E/N for which the ion energy distribution function has a negligible overlap in the energy range where charge transfer occurs. However, for the highest reduced electric field of $E/N = 150$ Td considered in this work, the ion energy distribution function (see Fig. 4) becomes negligible only above approximately 25 eV and the mean ion energy is about 3.5 eV in this case. Then, inelastic processes (nonresonant charge transfer and ion excitation) have to be taken into account in order to give accurate mobility results. To analyze the effects of inelastic processes on the cross section and mobility results, elastic collision cross sections were also calculated by using the electronic ground state $V_1(r, \varphi; r_{\text{fix}} = 2.1 \text{ a.u.})$ only, i.e., the

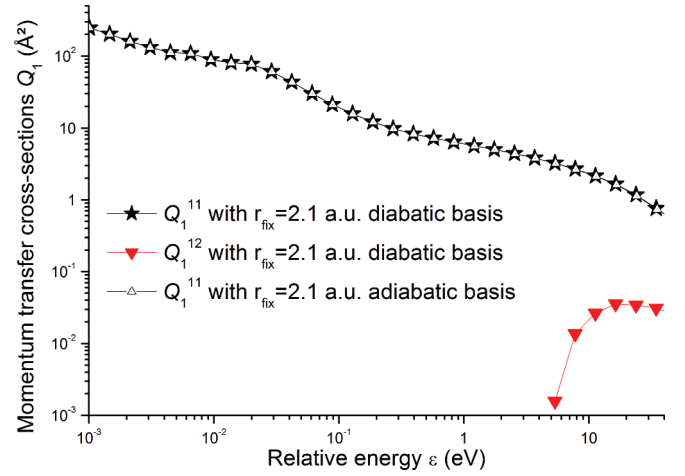


FIG. 3. (Color online) Quantum elastic $Q_1^{11}(\varepsilon; r_{\text{fix}} = 2.1 \text{ a.u.})$ and charge transfer $Q_1^{12}(\varepsilon; r_{\text{fix}} = 2.1 \text{ a.u.})$ momentum transfer cross sections for the He_2^+/He interaction system calculated from the Calvo's DIM interaction potential surfaces [9,10] in the diabatic basis. Elastic momentum transfer cross section was also calculated from the adiabatic basis using $V_1(r, \varphi; r_{\text{fix}} = 2.1 \text{ a.u.})$ only and shows no significant differences from the calculated one in the fully coupled diabatic basis.

adiabatic basis. In Fig. 3, we see that the elastic momentum transfer cross sections, calculated using either the diabatic or the adiabatic basis, are very similar. This means that inelastic processes have no significant effect on the calculated elastic collision cross section. This remains valid for all the He_2^+ frozen internuclear distances r_{fix} considered.

Reduced data for ion mobilities were calculated from the momentum transfer cross sections obtained from the two different calculations. In the case of the diabatic basis, elastic and inelastic momentum transfer cross sections have been used [6]. In the Monte Carlo simulation, inelastic processes lead to the disappearance of ions and then fictitious ionizations have been considered in order to reduce the statistical fluctuations [8]. Figure 5 shows the E/N dependence of the calculated reduced mobilities using the collision cross sections obtained for each basis set considered and compares them with the experimental mobility data compiled by Ellis *et al.* [13]. A clear

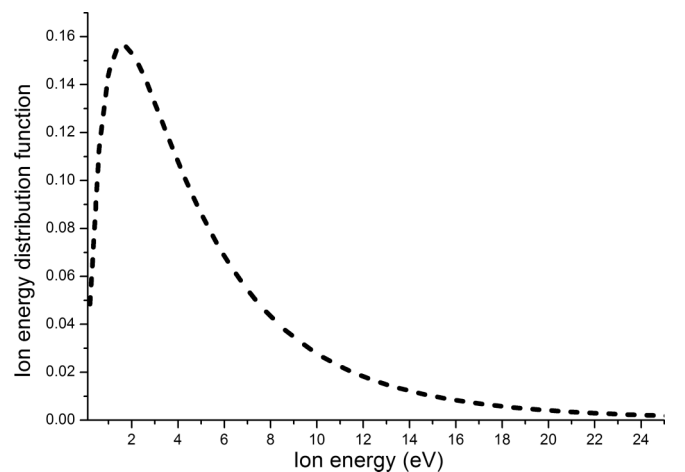


FIG. 4. He_2^+ ion energy distribution function for $E/N = 150$ Td.

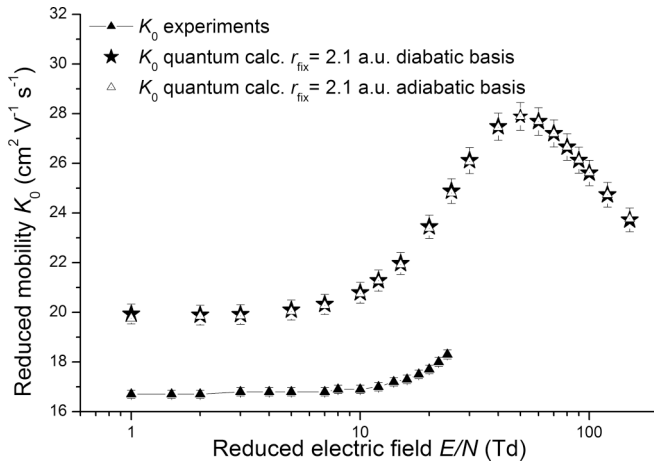


FIG. 5. Calculated mobilities with $\pm 2\%$ statistical error using the quantum method ($r_{\text{fix}} = 2.1$ a.u.) from the diabatic and adiabatic Calvo's DIM interaction potential surfaces [9,10]. Experimental mobilities [13] are also shown for comparison with error bars of 1%.

overestimation is observed. It is noteworthy that the diabatic calculation, which takes into account inelastic processes, gives a similar reduced mobility results as the adiabatic one. This means that charge transfer and ion excitation cross sections are not high enough to affect the ion transport coefficients for the considered energy range. This negligible effect of inelastic processes on mobility results remains valid also for all other frozen internuclear distances r_{fix} considered. The mobilities obtained with a frozen equilibrium distance $r_{\text{fix}} = 2.1$ a.u. presents a maximum value of $27.9 \text{ cm}^2 \text{ V}^{-1} \text{ s}^{-1}$ observed at 50 Td. Relative deviations from experimental mobility data are 18% at 1 Td and 32% at 20 Td.

As the second step, we tested the dependence of calculated collision cross sections and ion mobilities on calculation method. Since we showed that the ion transport coefficients can be obtained from momentum transfer cross sections calculated in the adiabatic basis, i.e., considering elastic processes only, the semiclassical method (JWKB) can also be used. Figure 6 shows the elastic momentum transfer cross section obtained with the semiclassical calculation for $r_{\text{fix}} = 2.1$ a.u. The differences between quantum and semiclassical results were investigated by a comparison of corresponding nonaveraged elastic momentum transfer cross sections, respectively $Q_1^{11}(\varepsilon; r_{\text{fix}}, \varphi)$ and $Q_{1,\text{JWKB}}^{11}(\varepsilon; r_{\text{fix}}, \varphi)$, for several approach angles φ . As noticed by Munn *et al.* [11], very small deviations due to the semiclassical approximation were observed for different relative collision energy ε . Collision energies where the deviations occur vary as a function of the approach angles φ considered for the cross section calculation. These small deviations lead to no significant differences between quantum and semiclassical mobilities are observed with relative deviations within the error bars (see Fig. 7).

B. Hybrid results

In order to improve the agreement between calculated mobilities and measured ones, hybrid calculations that take into account diatomic vibrational and rotational motions, were performed using Calvo's DIM model [9,10]. First,

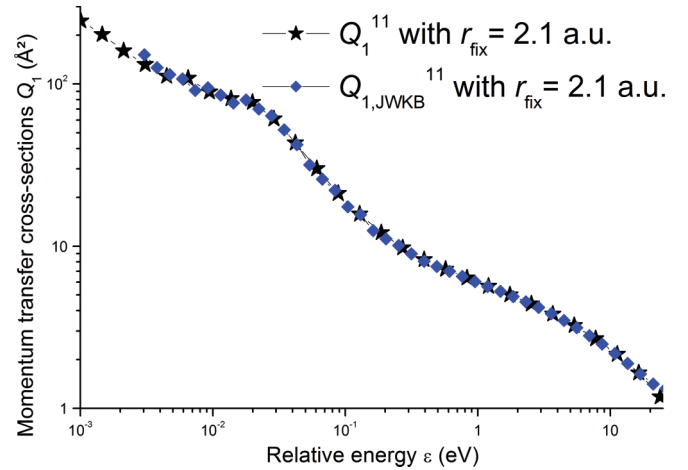


FIG. 6. (Color online) Quantum and semiclassical momentum transfer cross section for the He_2^+/He interaction system obtained using the IOS approximation with $r_{\text{fix}} = 2.1$ a.u. for a centre of mass energy range varying from 1 meV to 25 eV.

hybrid calculations were performed for the diatomic He_2^+ initially frozen at $r_{\text{fix}}^{\text{init}} = 2.1$ a.u. but then flexible along the collision trajectory. Figure 8 displays the obtained cross sections: $Q_{1,\text{hyb}}(\varepsilon)$, which contains elastic and electronic excitations, and the three-body dissociation cross section $Q_{0,\text{hyb}}^{\text{diss}}(\varepsilon)$. The quantum elastic momentum transfer cross section $Q_1^{11}(\varepsilon; r_{\text{fix}} = 2.1 \text{ a.u.})$ is also shown for comparison. In Fig. 8, we see that the hybrid $Q_{1,\text{hyb}}(\varepsilon)$ cross section obtained is larger than the quantum one up to about 5 eV (maximal relative difference being around 40%). Above this energy, the existence of the competing dissociative process decreases the cross sections of the nondissociative ones. However, this fall of the hybrid momentum transfer cross section can be compensated by explicitly including the dissociation channel in mobility calculations (see Fig. 9). Two basic observations are clear from this figure. Firstly, the hybrid mobility is smaller than the quantum one since the hybrid cross section, $Q_{1,\text{hyb}}^{(\varepsilon)} + Q_{0,\text{hyb}}^{\text{diss}}(\varepsilon)$, is

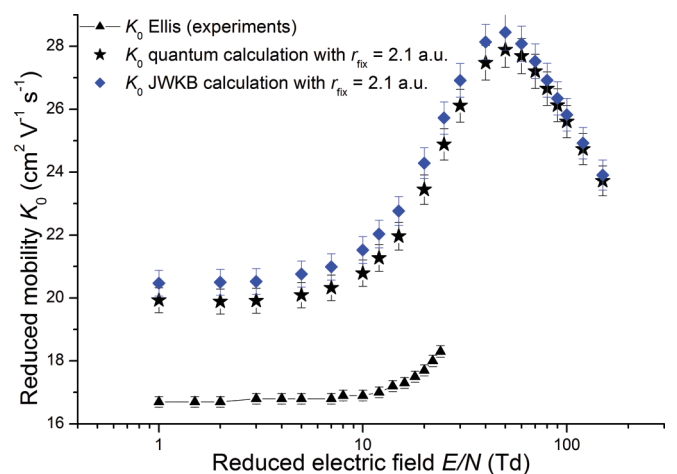


FIG. 7. (Color online) Comparison between experimental ion mobility [13] and the calculated ones from the Calvo's DIM interaction potential surfaces [9,10] using the quantum and the semiclassical methods with $r_{\text{fix}} = 2.1$ a.u.

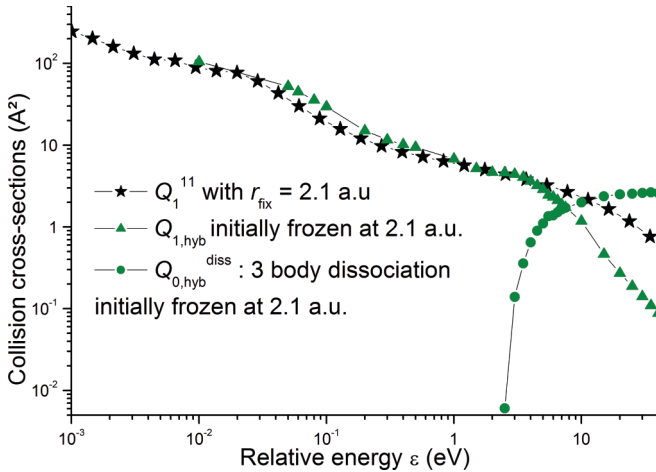


FIG. 8. (Color online) Hybrid collision cross sections for elastic and electronic excitations $Q_{1,hyb}$ and for three-body dissociation $Q_{0,hyb}^{diss}$ for He_2^+ initially frozen at $r_{fix}^{init} = 2.1$ a.u. compared to the quantum elastic momentum transfer cross section Q_1^{11} for the diatomic frozen at $r_{fix} = 2.1$ a.u.

larger than the quantum one, $Q_1^{11}(\epsilon; r_{fix} = 2.1 \text{ a.u.})$. Second, the inclusion of the dissociative channel allows us to obtain the expected bump in the E/N dependence of the ion mobility with a maximum of $K_0 = 22.5 \text{ cm}^2 \text{ V}^{-1} \text{ s}^{-1}$ at $E/N = 90$ Td. Monte Carlo simulations with and without the dissociation cross sections included, show that the mobility decrease at intermediate field is due to the collisional dissociation of the dimer. However, the hybrid mobility obtained for $r_{fix}^{init} = 2.1$ a.u. is below the experimental one and shows a constant relative deviation from the experimental data points of about 13%.

This deviation of the hybrid mobilities from the experimental data points can be attributed to the existence, in the present light molecular system, of strong quantum effects, which are not taken into account in the hybrid calculation. In order to correct hybrid collision cross sections, i.e., to effectively include the quantum effects, a hybrid calculation was performed under the same conditions as the quantum

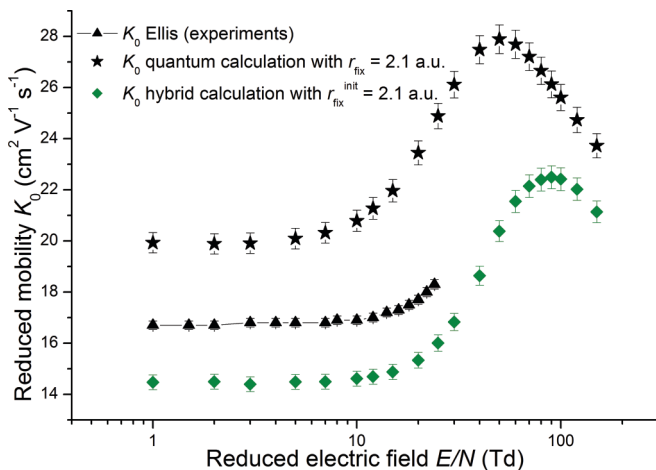


FIG. 9. (Color online) Measured ion mobilities [13] and calculated ones with 2% statistical error from the Calvo's DIM interaction potential surfaces [9,10] using the hybrid cross sections for $r_{fix}^{init} = 2.1$ a.u. and the quantum ones for $r_{fix} = 2.1$ a.u.

ones, i.e., with the diatomic frozen at $r_{fix} = 2.1$ a.u. along the whole collision trajectory. The only difference between the two calculations was that, in the frozen quantum calculation, the anisotropy of the atom-molecule interaction was taken into account by averaging over the approach angle φ , while in the rigid hybrid calculation the rotation of the molecule was allowed. Then, a correction factor, called quantum correction factor (QCF), was determined such that after it was applied to the rigid hybrid collision cross sections, the mobilities obtained via the Monte Carlo simulation were as close as possible to the frozen quantum ones. The correction factor was not defined as the ratio of the hybrid and quantum collision cross sections since the quantum method does not provide the cross section for the three-body dissociation. The corresponding rigid hybrid cross sections for collision energy varying from 0.01 eV to 40 eV are shown in Fig. 10(a). The elastic quantum collision cross section obtained for $r_{fix} = 2.1$ a.u. is also presented for comparison. We see in this figure that at low collision energies (in the range 0.03–1 eV), which correspond to the weak field region, the rigid hybrid cross section is larger than the quantum one while for high energies they are very similar. This leads to rigid hybrid mobilities with at most 20% deviation from the quantum ones at low electric field and comparable mobilities at high field [see Fig. 10(b)]. A quantum correction factor (QCF) varying between 0.78 and 1 [see Fig. 10(c)] was found to yield the best correspondence between quantum and corrected hybrid mobilities calculated for the dimer frozen at $r_{fix} = 2.1$ a.u. Then, the QCF was used to correct the hybrid mobilities as shown in Fig. 10(d). It is noteworthy that the QCF profile depicted in Fig. 10(c) becomes close to 1 at high energy. This reflects the fact that at high energy the De Broglie wavelengths and quantum effects become small.

This quantum correction factor can now be applied to the hybrid cross section shown in Fig. 8. The resulting corrected mobilities obtained from hybrid calculations are plotted against the electric field in Fig. 11. Noncorrected hybrid mobilities and experimental mobilities are also shown for comparison. The corrected mobility presents a maximum of $K_0 = 23.1 \text{ cm}^2 \text{ V}^{-1} \text{ s}^{-1}$ at 70–80 Td (in comparison with the uncorrected maximum mobility $K_0 = 22.5 \text{ cm}^2 \text{ V}^{-1} \text{ s}^{-1}$ at 90 Td) and a relative deviation between about 7% and 10% from the experimental results. This is a small improvement as compared to 13% error observed for the uncorrected hybrid mobilities. Notice however that, whereas uncorrected hybrid mobility is smaller than the experimental one, the corrected one is larger.

This systematic deviation of the theoretical prediction from the experimental data is probably due to the fact that the nuclear delocalization effects in the initial state of the system are neglected. These effects are very important in helium, which is light. Calculations considered so far assumed initially frozen dimers only. At the classical level, nuclear delocalization can simply be included by increasing the vibrational energy of the colliding dimer. We assume low temperatures and perform an additional hybrid calculation for the diatomic initially at the zero-point energy (ZPE) level. Figure 12 displays these new collision cross sections compared to the hybrid data obtained for initially frozen dimers. We see that the collision cross sections $Q_{1,hyb}$ (elastic processes and electronic excitations) and $Q_{1,hyb}^{diss}$ (three-body dissociation) for the dimer initially

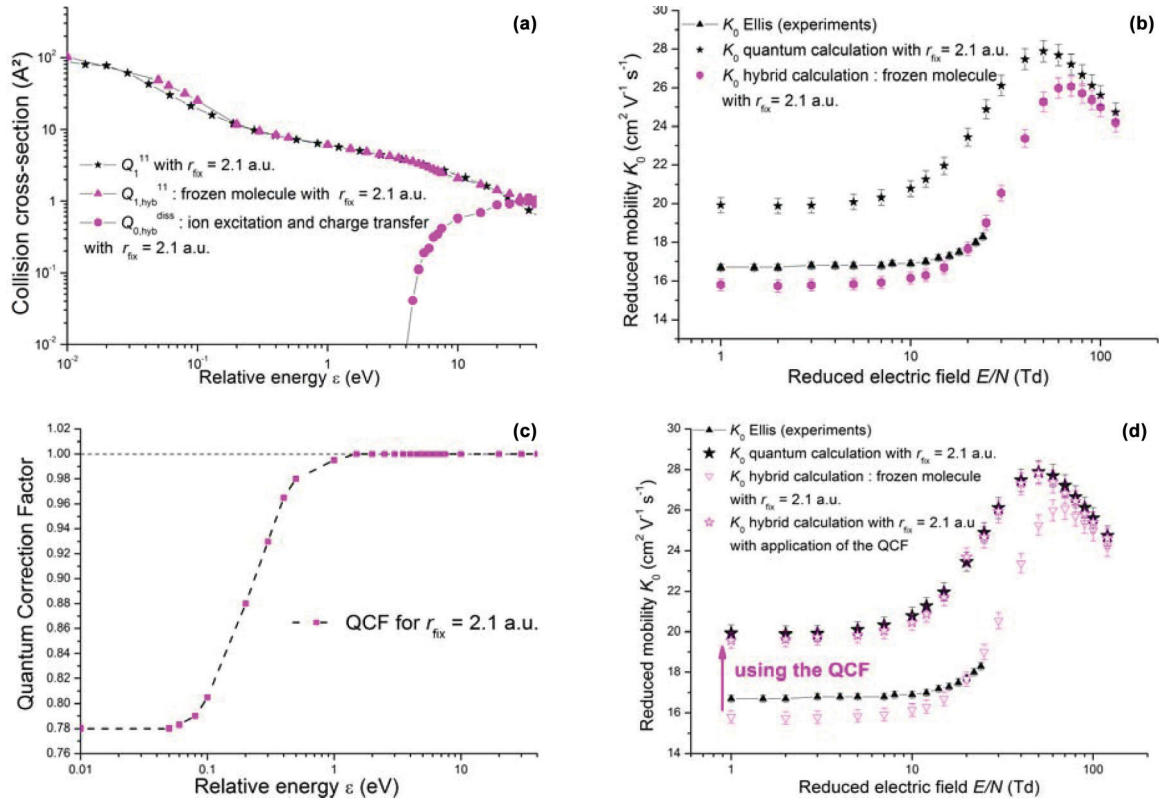


FIG. 10. (Color online) Hybrid and quantum (a) collision cross sections and (b) corresponding mobilities for He_2^+ frozen at $r_{\text{fix}} = 2.1$ a.u. without any correction. Mobilities obtained without and with the use the quantum correction factor (c) are shown in figure (d).

excited at ZPE is larger than the collision cross section obtained for He_2^+ initially frozen at $r_{\text{fix}} = 2.1$ a.u. Therefore, the mobility obtained for the ZPE excited diatom is smaller than the mobility of the initially frozen diatom (see Fig. 13). Using the quantum correction factor QCF, we obtain the mobility of He_2^+ ions initially excited at ZPE with the quantum effects implicitly included. The E/N dependence of the calculated reduced mobility for He_2^+ ions initially excited at ZPE is listed

in Table I and shown in Fig. 13 with a relative statistical error of $\pm 2\%$. Then, the corrected mobility presents a maximum of $K_0 = 21.9 \text{ cm}^2 \text{ V}^{-1} \text{ s}^{-1}$ at 60 Td and a relative deviation from experimental results between 4.7% and 6.0%.

Longitudinal and transversal diffusion characteristic energies, respectively eD_L/K and eD_T/K ($K = K_0N$), which are needed for multidimensional modeling of plasma jet electrodynamics, were also calculated. Figure 14 shows the

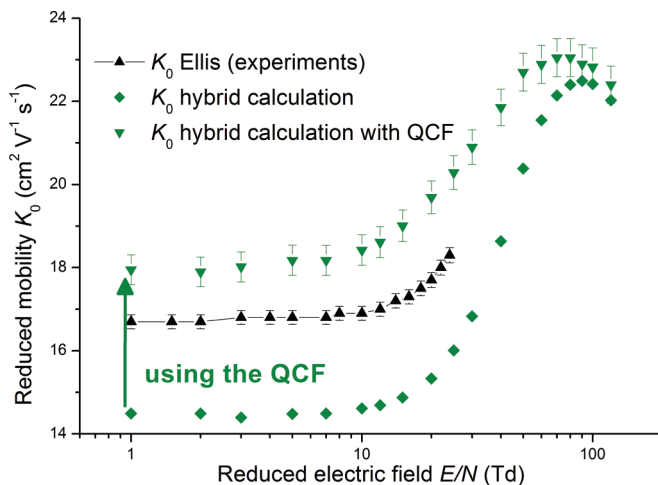


FIG. 11. (Color online) Corrected and non-corrected reduced mobilities calculated from the hybrid collision cross sections with $r_{\text{fix}}^{\text{init}} = 2.1$ a.u.

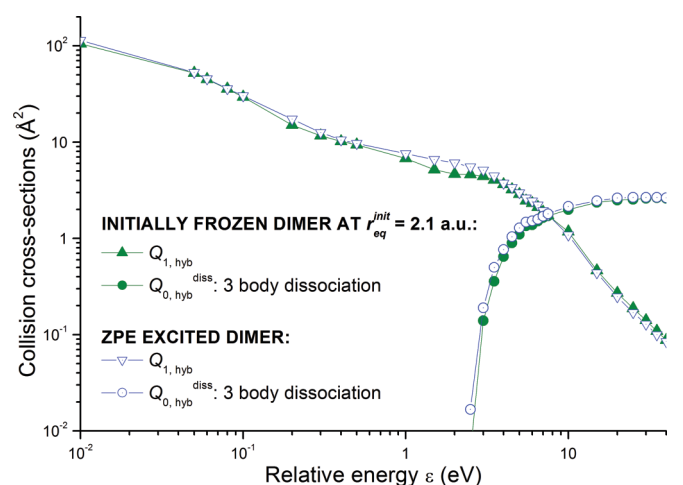


FIG. 12. (Color online) Hybrid collision cross sections for the He_2^+ ions initially frozen at 2.1 a.u. (green points) and He_2^+ initially excited at ZPE (blue points).

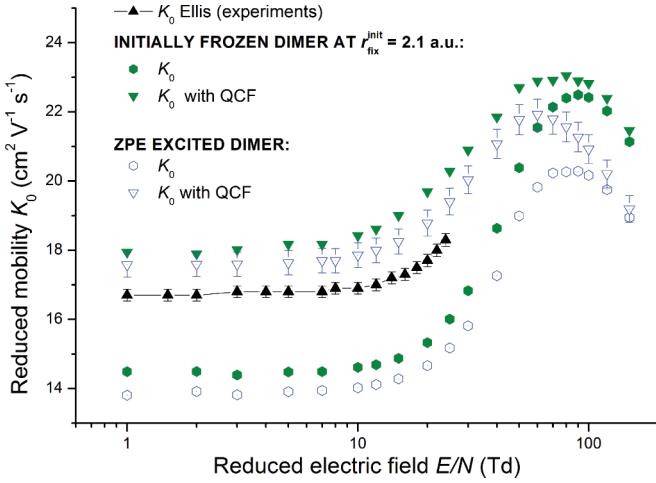


FIG. 13. (Color online) Hybrid mobilities obtained for the He_2^+ ions initially frozen at 2.1 a.u. (green points) and He_2^+ initially excited at ZPE (blue points) without (round) and with (triangles) the use of the QCF.

calculated longitudinal and transversal diffusion characteristic energy in meV plotted against the reduced electric field. Diffusion characteristic energies are also listed in Table II which shows that at $E/N = 1$ Td, longitudinal and transversal characteristic energy tend to 25.8 meV. This value is consistent with the one obtained from the Nernst-Townsend-Einstein relation [26] valid in weak fields,

$$eD/K = k_B T, \quad (3.1)$$

where k_B is the Boltzmann constant, T is the temperature, and e is the electric charge of the ion, for $T = 300$ K.

The characteristic energy curves show the typical shape for diffusion namely a plateau at low fields and then we observe an increase of D_L and D_T with the increase of the field, due to the decrease of the elastic momentum collision cross section.

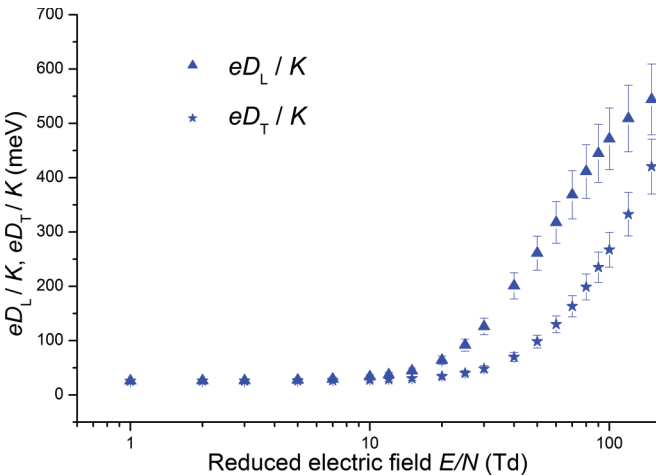


FIG. 14. (Color online) Longitudinal eD_L/K and transversal eD_T/K diffusion characteristic energies for He_2^+ in He. The dimers are excited at ZPE. eD_L/K and eD_T/K were plotted with a maximal relative statistical error of 12%.

TABLE I. Measured and calculated reduced mobility K_0 in $\text{cm}^2 \text{V}^{-1} \text{s}^{-1}$ of He_2^+ ions in He.

E/N (Td)	Experimental results ^a	Calculated K_0 (hybrid method ^b)	Calculated K_0 (inverse method ^c)
1	16.7 ± 0.2	17.5 ± 0.4	17.0 ± 0.3
2	16.7 ± 0.2	17.5 ± 0.4	17.0 ± 0.3
3	16.8 ± 0.2	17.6 ± 0.4	17.1 ± 0.3
5	16.8 ± 0.2	17.6 ± 0.4	17.1 ± 0.3
7	16.8 ± 0.2	17.7 ± 0.4	17.1 ± 0.3
8	16.9 ± 0.2	17.7 ± 0.4	17.1 ± 0.3
10	16.9 ± 0.2	17.9 ± 0.4	17.1 ± 0.3
12	17.0 ± 0.2	18.0 ± 0.4	17.2 ± 0.3
14	17.2 ± 0.2	18.2 ± 0.4	17.2 ± 0.3
15		18.3 ± 0.4	17.3 ± 0.3
16	17.3 ± 0.2	18.4 ± 0.4	17.3 ± 0.3
18	17.5 ± 0.2	18.6 ± 0.4	17.4 ± 0.3
20	17.7 ± 0.2	18.8 ± 0.4	17.6 ± 0.4
22	18.0 ± 0.2	19.0 ± 0.4	17.8 ± 0.4
24	18.3 ± 0.2	19.3 ± 0.4	18.0 ± 0.4
25		19.4 ± 0.4	18.2 ± 0.4
30		20.0 ± 0.4	18.9 ± 0.4
40		21.1 ± 0.4	20.0 ± 0.4
50		21.8 ± 0.4	21.2 ± 0.4
60		21.9 ± 0.4	21.9 ± 0.4
70		21.8 ± 0.4	22.2 ± 0.4
80		21.6 ± 0.4	22.1 ± 0.4
90		21.3 ± 0.4	21.9 ± 0.4
100		20.9 ± 0.4	21.6 ± 0.4
120		20.2 ± 0.4	20.7 ± 0.4
150		19.2 ± 0.4	19.5 ± 0.4
200			17.8 ± 0.4
300			15.5 ± 0.3
400			13.9 ± 0.3
500			12.8 ± 0.3

^aReference [13].

^b He_2^+ ions are initially excited at ZPE and the quantum correction factor was used.

^cMobility is calculated from a (12-4) core potential.

C. Extrapolation of transport coefficients from an effective potential

Finally, as the last step, an extrapolation method was used to reproduce first the experimental mobility data at low reduced electric field E/N and then to extend the calculated mobility at higher fields. Various extrapolation models have been used to describe the ion-atom interaction systems in order to get the corresponding ion transport data. Generally, calculated transport coefficients have been obtained in good agreement with experimental results using interaction potential models of Refs. [27] and [28]. It is noteworthy to emphasize a ($n-4$) core potential model is better adapted for a polyatomic ion interacting both with polar or nonpolar gases. The rigid core potential $V_{\text{core}}(r)$ can be written as [28]:

$$V_{\text{core}}(r) = \frac{n\epsilon_w}{3n-12} \left\{ \frac{12}{n} \left(\frac{r_m - a}{r - a} \right)^n - 3 \left(\frac{r_m - a}{r - a} \right)^4 \right\}, \quad (3.2)$$

TABLE II. Calculated longitudinal and transversal diffusion characteristic energy, respectively eD_L/K and eD_T/K , in meV.

E/N (Td)	eD_T/K (hybrid method ^a)	eD_L/K (hybrid method ^a)	eD_T/K (inverse method ^b)	eD_L/K (inverse method ^b)
1	25.8 ± 3.1	25.8 ± 3.1	25.9 ± 1.0	25.9 ± 1.0
2	25.9 ± 3.1	26.4 ± 3.2	25.7 ± 1.0	26.1 ± 1.0
3	26.0 ± 3.1	26.5 ± 3.2	26.2 ± 1.0	26.3 ± 1.1
5	26.4 ± 3.2	27.7 ± 3.3	26.2 ± 1.0	27.2 ± 1.1
7	26.9 ± 3.2	29.4 ± 3.5	26.8 ± 1.1	28.7 ± 1.1
10	27.7 ± 3.3	33.2 ± 4.0	27.6 ± 1.1	31.6 ± 1.3
12	28.6 ± 3.4	36.9 ± 4.4	28.4 ± 1.1	34.6 ± 1.4
15	30.2 ± 3.6	44.9 ± 5.4	29.8 ± 1.2	40.4 ± 1.6
20	34.5 ± 4.1	64.3 ± 7.7	33.2 ± 1.3	56.3 ± 2.3
25	40.3 ± 4.8	92.3 ± 11.1	38.2 ± 1.5	83.5 ± 3.3
30	48.1 ± 5.8	126.4 ± 15.2	45.6 ± 1.8	123.3 ± 4.9
40	70.1 ± 8.4	200.8 ± 24.1	67.4 ± 2.7	233.7 ± 6.4
50	98.2 ± 11.8	262.1 ± 31.4	97.8 ± 3.9	334.0 ± 13.4
60	129.0 ± 15.5	317.5 ± 38.1	133.3 ± 5.3	402.3 ± 16.1
70	163.5 ± 19.6	370.3 ± 44.4	172.6 ± 6.9	446.8 ± 1.6
80	198.6 ± 23.8	410.9 ± 49.3	213.3 ± 8.5	481.2 ± 19.2
90	234.8 ± 28.2	446.1 ± 53.5	256.7 ± 10.3	509.0 ± 20.4
100	269.6 ± 32.4	470.7 ± 56.5	298.1 ± 11.9	539.3 ± 21.6
120	334.3 ± 40.1	507.6 ± 60.9	383.9 ± 15.4	607.2 ± 24.3
150	417.9 ± 50.1	546.0 ± 65.5	517.0 ± 20.7	731.4 ± 29.3
200			748.7 ± 29.9	981.4 ± 39.3
300			1243.1 ± 49.7	1531.1 ± 61.2
400			1770.9 ± 70.8	2109.4 ± 84.4
500			2343.4 ± 93.7	2690.5 ± 107.6

^aHe₂⁺ ions are initially excited at ZPE and the quantum correction factor was used.

^bMobility is calculated from a (12-4) core potential.

where ε_w is the potential well depth, r_m the position of the potential minimum and r the internuclear distance. The rigid core diameter a , describes the shift of the center of mass from the charge center induced by the influence of the ion on the neutral atom. It is well known that the interaction potential for the interaction between ions and atoms presents a repulsive part at short internuclear distance r and an attractive part for larger r .

In the framework of this method, which we call the *inverse* method, potential parameters n , ε_w , a , r_m were adjusted until a good agreement is found between calculated and measured mobilities over the range of experimental reduced electric field [13]. Reduced mobilities were calculated from elastic momentum transfer cross sections determined from the semiclassical JWKB approximation (cf. Sec. II B 1) using the $(n-4)$ core interaction potential defined by Eq. (3.2). Then, the momentum collision cross section $Q_{1,(n-4)}$ was calculated over a wide range of center of mass energy. Using Monte Carlo simulation, the cross section provides calculated ion transport coefficients (K_0 , eD_L/K and eD_T/K) over a wide range of reduced electric field E/N .

Several sets of potential parameters n, ε_w, a , and r_m were tested for fitting the experimental data within the error bars. The unique solution set was found for: $n = 12, \varepsilon_w = 0.168$ eV, $a = 0.01$ Å and $r_m = 1.55$ Å. Indeed, many trials fitted the mobility plateau well, but were outside the errors bars in the region of rising experimental mobility. Figure 15 shows the cross section obtained from the (12-4) core potential. The

hybrid cross sections for diatomic helium ions initially excited at ZPE (with the use of the QCF) is also shown in this figure for comparison.

We see in this figure that the (12-4) core collision cross section is close to the sum of the hybrid cross sections $Q_{1,hyb}^{(\varepsilon)} + Q_{0,hyb}^{diss}(\varepsilon)$, except in the low ion relative energy region

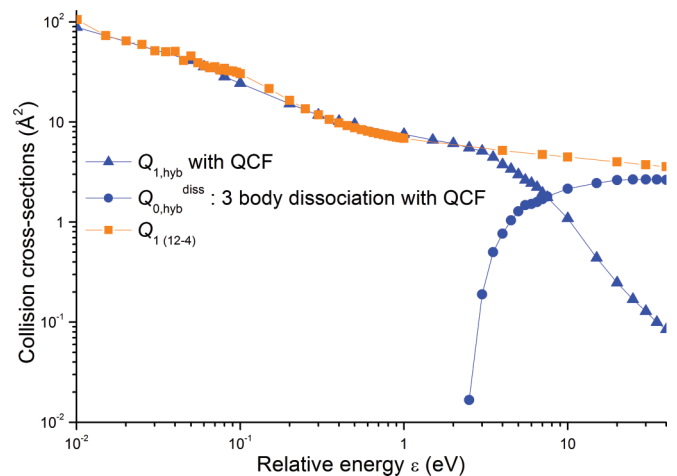


FIG. 15. (Color online) Collision cross section obtained from a (12-4) core potential and compared to hybrid collision cross sections for the He₂⁺ ions initially excited at ZPE with QCF.

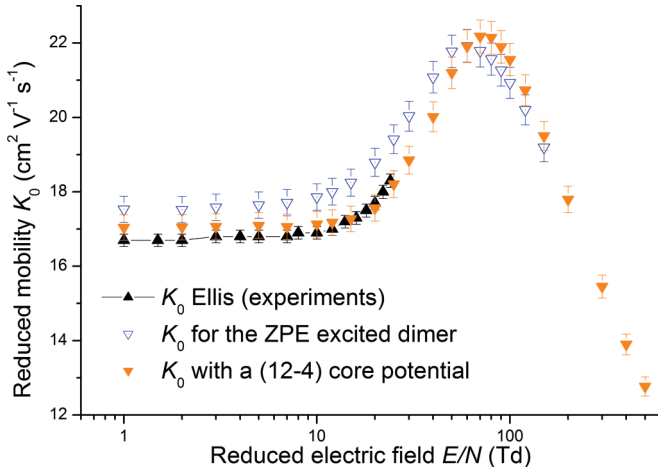


FIG. 16. (Color online) Mobilities obtained from a (12-4) core potential and hybrid mobilities obtained for the He_2^+ ions initially excited at ZPE with QCF.

around approximately 0.3 eV. These differences (up to 20%) lead to lower inverse method mobilities at low E/N , within the error bars of experimental data, as compared to those obtained with the hybrid method (see Fig. 16). However, from $E/N = 60$ Td, mobilities obtained from both methods are very similar and within their respective error bars ($\pm 2\%$). The inverse method, which uses spherical potential to describe the atom-molecule interaction He_2^+/He gives results (Fig. 16) in a quite surprisingly good agreement with the hybrid mobilities, accurately reproducing the maximum.

Moreover, longitudinal and transversal diffusion characteristic energies, eD_L/K and eD_T/K , were calculated with the inverse method up to 500 Td. These ion transport coefficients are shown in Fig. 17 and compared to the coefficients obtained with the hybrid method. A good agreement was obtained for the longitudinal and the transversal characteristic energies obtained using both methods within respectively a mean

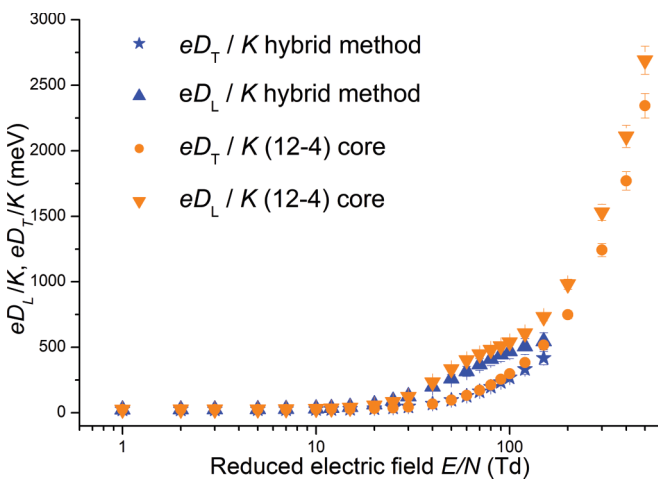


FIG. 17. (Color online) Longitudinal eD_L/K and transversal eD_T/K diffusion characteristic energies for He_2^+ in He obtained with a (12-4) core potential and with a hybrid method for particles initially excited at ZPE. Data were plotted with a maximal relative statistical error of 12% for the hybrid method and 4% for the inverse method.

relative error of 5% and 2.2% and a maximum relative error of 25.35% and 19.15% at 150 Td.

D. Discussions

The quantum method is exact in principle, however as a full three-dimensional (3D) calculation would be very difficult and outside the scope of the present contribution, we have performed approximations such as limitation to 1D calculation freezing the He^+/He distance and then averaging over angles. It leads to a clear overestimation of the mobility, and therefore to some underestimation of the collision cross sections. It should be emphasized that the equilibrium distance is the most probable one for the rather cold diatomics present in the cold plasma, thus this choice is reasonable.

On the other hand, the hybrid method does not suffer from this limitation and rotations as well as vibrations or even fragmentations are taken into account, however the nuclei follow a classical trajectory and their quantum effects are ignored. It leads to an underestimation of the mobility and therefore to some overestimation of the collision cross sections.

Notably, the experimental mobility results are bracketed by the quantum and the hybrid ones. This encourages us to take into account the quantum effects for the nuclei by a direct comparison of the hybrid and quantum calculations done in similar conditions and to the QCF correction that we have further applied to the unconstrained hybrid results.

It should also be noticed that the rigid core potential used with the semiclassical approach should not be considered as realistic but as an effective potential. Here, the diatomic is also frozen and moreover its interaction with the atom is represented by a spherical potential, which reproduces nicely the experimentally known mobilities and therefore captures the correct behavior of the collision cross sections. Interestingly, the extrapolated mobilities obtained by this approach and the ones obtained by the hybrid + QCF correction approach for the most realistic ZPE initial distribution, are in reasonably good agreement. This gives confidence in the present theoretical results.

It is worth emphasizing that the mobility calculations are very sensitive to the collision cross section data. The rather small differences between the cross sections obtained from the 1D quantum and the hybrid approaches lead to noticeable differences in the mobilities. For the He^+ mobilities in helium gas, we also found an important sensitivity and we could discriminate between the potentials since the 1D quantum approach used for the collision was exact in that case [6]. Here by taking advantage of the combination of various approaches (1D quantum, hybrid, and semiclassical), we could derive grounded cross sections and reliable extrapolated mobilities.

IV. CONCLUSIONS

Momentum transfer collision cross sections were calculated using quantum, semiclassical, and hybrid methods. By using these collision cross sections, ion mobility data were determined from Monte Carlo simulation with a relative statistical error of 2% in comparison to the calculations directly based on differential cross sections. Quantum and semiclassical

calculations of collision cross sections performed in the framework of the IOS approximation, i.e., for the diatomic helium ion frozen at the equilibrium distance $r_{\text{eq}} = 2.1$ a.u., produced similar mobility results with a minimum relative deviation from experimental results of 18%. Hybrid calculations performed for the diatomic helium ions (initially frozen at the equilibrium distance and then flexible along the collision trajectory) showed a constant relative deviation from the experimental data of nearly 13%. A quantum correction factor, determined in order to correct hybrid collision cross sections, was applied to collision cross sections for the diatomic initially excited at ZPE level in order to include nuclear delocalization effects in the initial state. A better agreement between calculated and measured mobility has been found in this case with a relative error from experimental data between 4.7% and 6%. Finally, an inverse method based on a (12-4) core spherical potential model has been used to fit experimental mobility data at low E/N and to extrapolate the mobility calculations at higher fields. A good agreement (within error bars) was found between mobilities

obtained from this inverse method and from the hybrid method reproducing accurately the maximum. Furthermore, a good agreement was also obtained for longitudinal and transversal coefficients calculated from both methods with a respective mean relative error of 5% and 2.2%.

ACKNOWLEDGMENTS

R. K. acknowledges financial support from the Operational Programme *Research and Development for Innovations* funded by Structural Funds of the European Union and the state budget of the Czech Republic (Grant No. CZ.1.05/1.1.00/02.0070) and from the Ministry of Education, Youth and Sports of the Czech Republic (Grants No. LM2011033, No. 7E12028, and No. MSM6198910027). R. K. further expresses his thanks to Jan Premus, Mendel Gymnasium, Opava, Czech Republic, for providing us his auxiliary codes for hybrid calculations. The hybrid calculations have been performed on the computers of the Supercomputing Centre of the VSB, Technical University of Ostrava.

-
- [1] M. Yousfi, O. Eichwald, N. Merbahi, and N. Jomaa, *Plasma Sources Sci. Technol.* **21**, 045003 (2012).
- [2] M. G. Kong, G. Kroesen, G. Morfill, T. Nosenko, T. Shimizu, J. Van Dijk, and J. L. Zimmermann, *New J. Phys.* **11**, 115012 (2009).
- [3] M. Yousfi, N. Merbahi, A. Pathak, and O. Eichwald, *Fundamental & Clinical Pharmacology* **27**, 1 (2013).
- [4] M. Laroussi, *IEEE Trans. Plasma Sci.* **37**, 714 (2009).
- [5] Y. Sakiyama and D. B. Graves, *J. Phys. D* **39**, 3451 (2006).
- [6] A. Chicheportiche, B. Lepetit, M. Benhenni, F. X. Gadea, and M. Yousfi, *J. Phys. B* **46**, 065201 (2013).
- [7] J. Barata and C. Conde, *Nucl. Instrum. Methods Phys. Res. A* **619**, 21 (2010).
- [8] M. Yousfi, A. Hennad, and O. Eichwald, *J. Appl. Phys.* **84**, 107 (1998).
- [9] F. Calvo, F. Y. Naumkin, and D. J. Wales, *J. Chem. Phys.* **135**, 124308 (2011).
- [10] F. Calvo, F. Y. Naumkin, and D. J. Wales (personal communication).
- [11] R. J. Munn, E. A. Mason, and F. J. Smith, *J. Chem. Phys.* **41**, 3978 (1964).
- [12] G. A. Parker and R. T. Pack, *J. Chem. Phys.* **68**, 1585 (1978).
- [13] H. W. Ellis, R. Y. Pai, E. W. McDaniel, E. A. Mason, and L. A. Viehland, *At. Data Nucl. Data Tables* **17**, 177 (1976).
- [14] F. O. Ellison, *J. Am. Chem. Soc.* **85**, 3540 (1963).
- [15] F. X. Gadea and I. Paidarová, *Chem. Phys.* **209**, 281 (1996).
- [16] P. J. Knowles, J. N. Murrell, and E. J. Hodge, *Mol. Phys.* **85**, 243 (1995).
- [17] P. J. Knowles and J. N. Murrell, *Mol. Phys.* **87**, 827 (1996).
- [18] M. Ovchinnikov, B. L. Grigorenko, K. C. Janda, and V. A. Apkarian, *J. Chem. Phys.* **108**, 9351 (1998).
- [19] M. Child, *Molecular collision theory* (Dover Publications, Mineola, NY, 1996).
- [20] R. De Vogelaere, *J. Res. Natl. Bur. Std.* **54**, 119 (1955).
- [21] I. Janeček, D. Hrivňák, R. Kalus, and F. X. Gadea, *J. Chem. Phys.* **125**, 104315 (2006).
- [22] I. Janeček, S. Cintavá, D. Hrivňák, R. Kalus, M. Fárník, and F. X. Gadea, *J. Chem. Phys.* **131**, 114306 (2009).
- [23] <http://moldyn.vsb.cz/index.php/software-menu/2-uncategorised/5-multidyn>
- [24] M. Yousfi, A. Hennad, and A. Alkaa, *Phys. Rev. E* **49**, 3264 (1994).
- [25] M. Benhenni, J. de Urquijo, M. Yousfi, J. L. Hernandez-Ávila, N. Merbahi, G. Hinojosa, and O. Eichwald, *Phys. Rev. E* **71**, 036405 (2005).
- [26] P. Watts and A. Wilders, *Int. J. Mass Spectrom.* **112**, 179 (1992).
- [27] E. A. Mason and E. W. McDaniel, in *Transport Properties of Ions in Gases* (Wiley-VCH, Weinheim, 2005).
- [28] E. A. Mason, H. O'Hara, and F. J. Smith, *J. Phys. B* **5**, 169 (1972).